# Causes of East Asian temperature multidecadal variability since AD 850

Jianglin Wang[1], Bao Yang[1], Timothy J. Osborn[2], Fredrik Charpentier Ljungqvist[3,4,5], Huan Zhang[6], and Jürg Luterbacher[6,7]

[1]Key Laboratory of Desert and Desertification, Northwest Institute of Eco-Environment and Resources, Chinese Academy of Sciences, Lanzhou, China

[2]Climatic Research Unit, School of Environmental Sciences, University of East Anglia, Norwich, United Kingdom

[3]Department of History, Stockholm University, Stockholm, Sweden

[4]Bolin Centre for Climate Research, Stockholm University, Stockholm, Sweden

[5]Department of Geography, University of Cambridge, Cambridge, United Kingdom

[6]Department of Geography, Climatology, Climate Dynamics and Climate Change, Justus Liebig University of Giessen, Giessen, Germany

[7]Centre of International Development and Environmental Research, Justus Liebig University of Giessen, Giessen, Germany

Corresponding author: Jianglin Wang (wangjianglin2011@lzb.ac.cn)

**Key Points:**

- Atlantic and Pacific Multidecadal Oscillations (AMO and PMO) are important contributors to East Asian temperature variability.
- The combined contribution of the AMO and PMO is of similar magnitude as solar and volcanic forcing during 850–1999.
- The most important drivers change between sub-periods: for 950–1250 it is the PMO, for 1350–1850 it is solar forcing.



This article has been accepted for publication and undergone full peer review but has not been through the copyediting, typesetting, pagination and proofreading process which may lead to differences between this version and the Version of Record. Please cite this article as doi: 10.1029/2018GL080725

**Abstract**

The drivers of multidecadal to centennial-scale variability in East Asian temperature, apparent in temperature reconstructions, are poorly understood. Here, we apply a multivariate regression analysis to distinguish the influences of large-scale modes of internal variability (Atlantic Multidecadal Oscillation, AMO; and Pacific Multidecadal Oscillation, PMO), and external natural (orbital, solar and volcanic) and anthropogenic (greenhouse gas concentrations, aerosols, and land use changes) forcings on East Asian warm-season temperature over the period 850–1999 AD. We find that ~80% of the temperature change on timescales longer than 30 years can be explained including all drivers over the full-length period. The PMO was the most important driver of multidecadal temperature variability during the Medieval Climate Anomaly (here, 950–1250), while solar contribution was important during the Little Ice Age (here, 1350–1850). Since 1850, two-thirds of temperature change can be explained with anthropogenic forcing, whereas one-third was related mainly to the AMO and volcanic forcing.

**Plain Language Summary**

The Atlantic Multidecadal Oscillation (AMO) and Pacific Multidecadal Oscillation (PMO) are suggested to be key components of internal temperature variability globally and in the Northern Hemisphere (NH). However, the contribution of the AMO and PMO to temperature at regional/continental scales in preindustrial times is still unclear. Here, we use a multivariate regression analysis to distinguish the AMO and PMO contributions to the East Asian temperature multidecadal (> 30 years) changes from the influence of external (orbital solar, volcanic, and anthropogenic) forcings. We find that the contribution of the AMO and PMO is of similar magnitude as solar and volcanic forcing during the period 850–1999 AD. We apply the same approach to three subperiods, and find that the PMO, solar forcing and anthropogenic forcing contributed most during the periods 950–1150, 1350–1850 and 1850–1999, respectively.

## 1. Introduction

Most of the increase in the global temperature observed since the mid-20th century was caused by external radiative forcings, especially by a rapid increase of anthropogenic greenhouse gases (Bindoff *et al.*, 2013). However, variations in the rate of warming (e.g. early 20$^{th}$ century warming, 1950s–1970s cooling and the slower rate of warming from 1998–2013) cannot be fully explained by anthropogenic forcing, and contributions from internal climate variability need to be taken into consideration (Lean and Rind, 2008; Folland *et al*., 2013; Steinman *et al.*, 2015; Meehl *et al.*, 2016; Hegerl *et al.*, 2018; Folland *et al*., 2018). The role of internal variability tends to be larger at continental/regional scales and on shorter timescales and decreases in importance at hemispheric and on longer longer timescales (Hawkins and Sutton, 2009).

Multidecadal variations of sea surface temperature (SST) in the North Atlantic (Atlantic Multidecadal Oscillation, AMO) and North Pacific (Pacific Multidecadal Oscillation, PMO) are key components of internal temperature variability even at global and Northern Hemisphere (NH) scales (Dai *et al.*, 2015; Steinman *et al.*, 2015; Cheung *et al.*, 2017; Wang *et al.*, 2017). The AMO and PMO represent a large proportion (~80%) of the NH temperature internal variability at lower (e.g., > 30 years) frequency since 1850 (Steinman *et al.*, 2015; Cheung *et al.*, 2017). The slower rate of global warming during 1998–2013 might be partly explained by a combined effect of a negative PMO phase and a modest positive AMO phase (Steinman *et al.*, 2015; Meehl *et al.*, 2016). Their combined effect over the 20th century and early 21st century, however, is relatively minor compared to the anthropogenic radiative forcing (Stolpe *et al.*, 2017).

The increasingly strong anthropogenic forcing during the instrumental period makes it challenging to isolate internal climate variability from external forcing and to identify the specific roles of the AMO and PMO. In this study, we expand such analyses beyond the instrumental period by using millennium-long proxy-based temperature reconstructions in tandem with observational evidence to carry out detection and attribution (D&A) studies

(Lean and Rind, 2008; Hegerl and Zwiers, 2011; Bindoff *et al.*, 2013; Schurer *et al.*, 2013; Schurer *et al.*, 2014) during the period 850–1999. Studies using D&A with temperature reconstructions have been limited to decadal-scale changes of the Northern Hemispheric and European mean temperature (Hegerl *et al.*, 2007; Hegerl *et al.*, 2011; Schurer *et al.*, 2013; Schurer *et al.*, 2014). Zhang *et al.* (2018) provide a new, 2000-year-long, multi-proxy East Asian warm-season temperature reconstruction and found an important role of internal variability and external forcing on multidecadal timescales but without conducting a formal D&A exercise.

Here, we use seven published East Asian temperature reconstructions together with climate forcing reconstructions to carry out a formal D&A study during the period 850–1999. We use a multiple linear regression-based approach similar to Lean and Rind (2008) and Wang *et al.* (2017) to detect the signals of external radiative drivers and the influences of specific modes of internally-generated variability, namely the AMO and PMO. We then attribute warm-season temperature changes over East Asia to a combination of individual factors. In particular, we examine the contribution of AMO and PMO to temperature changes during the Medieval Climate Anomaly (MCA), the Little Ice Age (LIA), and the Current Warm Period (CWP).

## 2. Data and Methods

### 2.1 Temperatures reconstructions and their composite

We selected seven reconstructions that extend at least the full past millennium and have a temporal resolution of 10 years or finer (Yang *et al.*, 2002; Wang *et al.*, 2007; Shi *et al.*, 2012; Cook *et al.*, 2013; Ge *et al.*, 2013; Shi *et al.*, 2015; Zhang *et al.*, 2018) (Table S1). The seven temperature reconstructions all exhibit significant variability at multidecadal timescales, with dominant periodicities ranging from ~32 to ~64 years (Figure S1). These reconstructions share a portion of proxy records, but were performed using different reconstruction/calibration approaches (see Zhang *et al.* (2018) for a detailed discussion about the proxies used, their spatial distribution, representativeness and validation of each

reconstruction). The seven reconstructions actually reflect various seasonal temperature signals (e.g., summer vs. annual). However, all reconstructions are to a large extent based on tree-ring records that more commonly record growing (warm) season climate (Wilson *et al*., 2016; Anchukaitis *et al*., 2017).

The seven reconstructions were 30-year low-pass filtered using a smoothing method in Mann (2008) to extract the "true smoothed behavior" for the part near boundaries of time-series. The filtered reconstructions were normalized to zero mean and unit standard deviation (SD) over their full period of overlap (1000–1989 AD), and then the composite mean and ±1 SD uncertainty range of the seven reconstructions were calculated for each year.

We used instrumental data for the extended warm-season (April–September) mean temperature of East Asia (10–55°N, 60–150°E) from the CRUTS4.01 dataset (Harris *et al.*, 2014). Like the temperature reconstructions, the instrumental data was smoothed using a 30-year low-pass filter. The composite of temperature reconstructions matches well with the instrumental record during the period 1901–1999 ($r$ =0.96, effective degrees of freedom ($N_{eff}$) = 6.6, $p$ <0.001; Figure. 1c). The $N_{eff}$ is calculated using the method described in Wang *et al*. (2017), by dividing the length of the time-series (e.g., 99 for 1901–1999) by the half of the length of the smoothing window (e.g., 30/2 here). The final composite reconstruction was developed by adjusting the mean and standard deviation to be the same as the instrumental record over the overlap period 1901–1999 (whose standard deviation is 0.18 °C).

**2.2 Climate forcing reconstructions**

We used a combination of reconstructions for well-mixed greenhouse gases ($CO_2$, $CH_4$ and $N_2O$; Schmidt *et al.*, 2012), land cover change (Kaplan *et al.*, 2010) and tropospheric aerosols (Miller *et al.*, 2014) to represent the anthropogenic forcing (Figure S2). The orbital forcing is the changes in April-September mean insolation at 40°N (Berger, 1978). The solar forcing dataset is from Steinhilber *et al.* (2009). The volcanic forcing is a global volcanic aerosol deposition reconstruction from sulfur records in both polar ice sheets (Sigl *et al.*, 2015).

However, our results do not alter much by using alternative solar and volcanic reconstructions (Figure S3).

### 2.3 The AMO and PMO reconstructions

We used the AMO reconstruction from Wang *et al.* (2017), which was estimated by removing an estimate of the externally forced component from the full reconstructed variance of North Atlantic SST (averaged over 80° W– 0° E, 0° N–70° N), an approach we will use to isolate internal variability of East Asian temperatures later (see "Multiple linear regression approach for detection and attribution"). We also isolated the PMO from the SST reconstruction of the North Pacific region (averaged over 22.5° N–57.5° N, 152.5° E–132.5° W; Mann et al., 2009) using a same approach as in the AMO and East Asian temperature internal variability (Figure S5). The PMO definition used here is consistent with Steinman *et al.* (2015), but different to the Pacific Decadal Oscillation, as the former is defined by removing the estimate of forced variability from the North Pacific area-mean SST whereas the latter is defined as the leading mode of the empirical orthogonal function (EOF) analysis on the North Pacific SST (in which the mean global SST anomaly has been subtracted from each grid point). Since most of the North Pacific region shows negative loadings in the EOF-based PDO index (Newman *et al*., 2016), the North Pacific area-mean SST and its internal variability (i.e., the PMO defined here) should be negatively correlated with the EOF-based PDO index.

We used only the internal variability components of the Atlantic and Pacific SST reconstructions (i.e., the AMO and PMO) (Steinman *et al.*, 2015; Wang *et al.*, 2017) to avoid the risk of overestimating the contributions from the two ocean basins due to a common response of temperature and SST to external forcing (Frankcombe *et al.*, 2015; Steinman *et al*., 2015; Cheung *et al.*, 2017; Wang *et al.*, 2017).

It should be noted that the PMO reconstruction shares a number of predictors with the seven East Asian temperature reconstructions, as Mann et al. (2009) included some East Asian proxy records to obtain spatial temperature field reconstructions across the globe, from which

the North Pacific SST was calculated. The AMO and all the climate forcing reconstructions, however, are independent and do not share any common predictors with individual temperature reconstructions.

We did not include the Mann *et al*. (2009) North Atlantic SST reconstruction because, especially prior to AD 1600, it is not independent from their PDO reconstruction, which we do use. This lack of independence would prevent us from adequately separating the influences of AMO and PMO. This may also indicate large uncertainty in their AMO reconstruction before AD 1300 when significant multidecadal variability seen in the reconstruction of Wang *et al*. (2017) is absent (figure S13–15 of Wang *et al*. 2017); the correlation between the two reconstructions is only 0.17 for 850–1299, but increases to 0.60 after 1300. For North Pacific, there is no any other SST reconstruction with a high resolution extending back to 850. An alternative reconstruction is for the PDO in MacDonald and Case (2005), covering the period 993–1996 and based on two site tree-ring records from North America; however; the two site tree-ring records of MacDonald and Case (2005) had also been included in the large proxy network of Mann *et al*. (2009), thus we did not include this reconstruction in our analyses too.

**2.3 Multiple linear regression approach for detection and attribution**

Multiple linear regression (MLR) has been widely used in D&A studies (Lean and Rind, 2008; Folland *et al*., 2013; Imbers *et al.*, 2013; Zhou and Tung, 2013; Chylek *et al.*, 2016; Wang *et al.*, 2017; Folland *et al*., 2018). Here, we apply MLR to detect and attribute past Asian extended warm-season temperature changes since AD 850. Before performing the MLR, all predictor variables were smoothed using a 30-year low-pass filter and normalized to obtain a zero mean and unit SD. For the given time *t*, the 30-year smoothed East Asian temperature (EAT) was estimated as:

$$\mathrm{EAT}(t) = \beta_0 + \beta_1 \mathrm{Ant}(t) + \beta_2 \mathrm{Orb}(t) + \beta_3 \mathrm{Sol}(t - \Delta t_{\mathrm{Sol}}) + \beta_4 \mathrm{Vol}(t - \Delta t_{\mathrm{vol}}) + \mathrm{Residual}(t)\,, \quad (1)$$

We consider four external radiative drivers, including anthropogenic (Ant), orbital (Orb),

solar (Sol), and volcanic (Vol) forcing. For solar and volcanic forcings, we permit a lagged time series to obtain the highest correlation (Knudsen *et al.*, 2014; Wang *et al.*, 2017). In this case, the lags are $\Delta t_{Sol}$ = 2 years and $\Delta t_{Vol}$ = 11 years for solar and volcanic forcing, respectively, though the cross-correlations vary only slightly for lags that are a few years more or less than this (*Figure S6*).

The scaling factors, $\beta$, and their standard errors were estimated using ordinary least squares. The signal of a particular forcing is considered to be detectable only if its scaling factor is significantly larger than zero (Schurer *et al.*, 2013). Only those forcing factors with detectable signals of the a priori expected sign (i.e. positive) were used to estimate the attributable temperature changes (by multiplying an individual forcing by its $\beta$ value). If the lower limit of a scaling factor' 95% confidence range includes zero then that scaling factor is set to zero. This causes only small differences in the results compared to including all forcings (i.e. even those whose scaling factors are not significant). The residual variability in equation (1) is our main estimate of internal variability (Steinman *et al*., 2015; Wang *et al*., 2017).

The analysis was extended to include to particular components of internal variability that operate on large scales by including reconstructed time-series of the AMO and PMO as additional predictor variables in the MLR:

$$\mathrm{EAT}(t) = \beta_0 + \beta_1 \mathrm{Ant}(t) + \beta_2 \mathrm{Orb}(t) + \beta_3 \mathrm{Sol}(t - \Delta t_{\mathrm{Sol}}) + \beta_4 \mathrm{Vol}(t - \Delta t_{\mathrm{vol}}) + \beta_5 \mathrm{PMO}(t) + \beta_6 \mathrm{AMO}(t) + \mathrm{Residual}(t), \quad (2)$$

As above, we used smoothed and normalized time-series for all predictor variables and only retained significantly positive $\beta$ to multiply climate drivers. This means that the contribution of each forcing to East Asian temperature changes is proportional to its scaling factor, $\beta$, and the "explained variance" (EV) for an individual climate forcing is calculated as:

$$\mathrm{EV}_i = 100\% \cdot \frac{\beta_i R^2}{\sum_{i=1}^{6} \beta_i}, \quad (3)$$

where $R^2$ is the coefficient of determination using all climate drivers; $i$, with a value from 1 to

6, means anthropogenic, orbital, solar, volcanic forcing, PMO and AMO, respectively.

Our main results were obtained by applying the MLR to the composite reconstruction of seven East Asian temperature reconstructions. We also repeated the analysis using individual temperature reconstructions, and calculated the ±1 SD ranges to assess the uncertainty range when using different reconstructions. To do this, all individual reconstructions had been rescaled to the CRU temperature over the period 1901–1999. In addition, the MLR approach was not only performed for the full period 850–1999, but also for three subset intervals: MCA (950–1250), LIA (1350–1850) and CWP (1850–1999) separately.

## 3. Results

### 3.1. East Asian temperature multidecadal variability

The seven millennial-long temperature reconstructions exhibit strong similarity on the longest (e.g., centennial and multicentennial) timescales, such as the generally positive anomalies from 950 to 1100 and after about 1900, and the generally negative anomalies from 1450 to 1700 (Figure 1a, b). The agreement on multidecadal time-series differs between periods though the correlations between each individual series and the composite of the others averages above 0.5 since 1700 AD, above 0.4 since 1600 AD and is close to 0.3 for the rest of the period.

The correlations between the individual reconstructions over the common period they shared range from $r$ = 0.20 to 0.80, with a median value of $r$ = 0.61 (Table S2). The reconstruction of Shi *et al.* (2015) has the highest correlation ($r$ = 0.84) with the composite of other six reconstructions (Table S2, S3), presumably because it has the largest proxy network and includes a higher proportion of proxy records that are common with others. The reconstruction of Cook *et al.* (2013) shows the lowest correlation ($r$ = 0.52) with the composite of the other reconstructions, likely because this reconstruction uses tree-ring records alone whereas the others are multi-proxy based. For a detailed discussion about the similarities and differences among the various reconstructions the reader is referred to Zhang

*et al.* (2018).

The generally good agreement among the reconstructions makes it reasonable to use a composite of them to represent their common expression of East Asian temperature variations. Like the individual reconstructions, the composite reconstruction shows a warm MCA and CWP, and a cold LIA (Figure 1c). The warmest conditions occurred in the end of the 20th century, whereas the coldest conditions occurred in the middle of the 17th century, consistent with the findings from Europe and the NH (Ljungqvist *et al.*, 2016; Luterbacher *et al.*, 2016).

### 3.2. The role of external forcing

To construct the regression model, we consider external forcings used in climate models (anthropogenic, orbital, solar, and volcanic). This set of predictors account for ~76% of temperature variance at multidecadal timescales since AD 850 (Figure 2a and Table S4). If orbital forcing is excluded from the set of predictors, there is a significant ($p < 0.05$) long-term cooling trend in the residuals (differences between the reconstructed and regressed temperature). This suggests that orbitally-forced cooling, usually reported in high northern latitude regions (Kaufman *et al.*, 2009; Esper *et al.*, 2012), might also contribute to a long-term cooling trend over East Asia. A significant contribution of anthropogenic forcing (which here includes pre-industrial variations in forcing agents, which might not be entirely anthropogenic in origin) is found since 1850, and to a lesser extent during the LIA, due to a combined effect of variations in greenhouse gases and land use (Figure 2b, *S2a*, and Table S4). In addition, we found minor contributions of solar and volcanic forcing compared to anthropogenic and orbital forcing for the full length period of 850–1999. This finding is insensitive to what solar and volcanic reconstructions are used (Figure S3).

The same multivariate regression analyses for the MCA, LIA and CWP separately yield slightly different results. The external radiative forcings account for most of the recent warming during the CWP, but are insufficient to account for the majority of the temperature change during the LIA and especially during the MCA. During the MCA volcanic forcing is

only detected, but it accounts for only ~6% of the temperature variance (Figure 2b, c, and Table S4). During the LIA, solar, volcanic and anthropogenic forcings can be significantly detected, however they share only ~35% of the temperature variance (Figure 2b, d, and Table S4). The residual temperature variance points to a substantial contribution from internal climate variability.

### 3.3. The role of internal variability, PMO and AMO

The internal variability of East Asian temperature, calculated by removing the externally-forced component, shows persistent multidecadal variations since AD 850 (Figure S7). It also shares similar multidecadal behaviors with the AMO and PMO, suggesting an association with the AMO and PMO (D'Arrigo and Wilson, 2006; Li *et al.*, 2008; Wang *et al.*, 2013; Wang *et al.*, 2015; Fang *et al.*, 2017; Luo *et al.*, 2018). As *Figure 3* shows, when adding the PMO and AMO to the set of the explanatory variables, the explained temperature variance increases from ~75% to ~80% for the full period 850–1999, with the largest increase during the MCA (from ~6% to ~30%), modest increases during the LIA (from ~35% to ~38%) and during the CWP (from ~93% to ~96%). The PMO and AMO contributed similar portions (~6% *vs.* ~5%) of multidecadal temperature changes for East Asia over the full length period 850–1999, but played different roles in the sub-periods (i.e., the MCA, LIA and CWP; Figure 4 and Table S5).

During the MCA, the PMO and volcanic forcing are important drivers, with a contribution of ~30% of temperature variance during the MCA (Figure 3c, 4, S8b, and Table S5). During the LIA, solar forcing is most important and accounts for ~14% of the temperature variance, while orbital, volcanic, anthropogenic forcing, AMO and PMO are also detected, but each contributes less than 7% (Figure 3d, 4, S8c, and Table S5). During the CWP, anthropogenic forcing accounts for two-thirds of the temperature variance since 1850, while the AMO and volcanic forcing together contribute one-third (Figure 3e, 4, S8d, and Table S5). If we use the MLR results from the full period and analyze them and calculate contributions over each sub-period, rather than using the MLR for each sub-period separately, the explained

temperature variance for each sub-period is slightly less, but the main findings are still hold (Figure S9). For example, we found that the PMO, solar and anthropogenic forcings are still the most important factors during the MCA, LIA and CWP, respectively.

## 4. Discussion and Conclusions

In this study, we confirm that the AMO and PMO are important forcing factors of multidecadal temperature variability in East Asia since AD 850. We found ~80% of the temperature variance explained by external drivers and the AMO and PMO. The high fraction of variance explained is striking given that our results are based on proxy-based reconstructions that are subject to uncertainties from a number of sources, i.e., possible time-varying climate-proxy relationships and potential spectral biases in some of the proxy types (Ljungqvist *et al.*, 2016). For the period 850–1999, we found that anthropogenic and orbital forcing significantly contributes to long-term of temperature variations, but the effect of solar and volcanic forcing, especially for the latter, is minor on the timescales considered here. The minor signal of volcanic forcing might also be partly related to the fact that part of the volcanic signal is possibly already "averaged out" in some individual reconstructions with a decadal resolution. Nevertheless, the minor contribution of volcanic forcing found here is in disagreement with findings for the NH mean temperature in model simulations (Atwood *et al.*, 2016; Otto-Bliesner *et al.*, 2016). This might partly be due to different responses of volcanic effect in reconstructions and model simulations (Hartl-Meier *et al.*, 2017) and also possibly in differences between East Asia and the NH (PAGES 2k consortium, 2013).

With a contribution of two-thirds of the temperature variance, external forcing is found to mainly control temperature changes in East Asia since 850. This contribution of external forcing is larger than that found in North Atlantic (Wang *et al.*, 2017) and in its surrounding regions, e.g., Europe (Luterbacher *et al.*, 2016), where the changes in ocean circulation and the interactions between atmosphere and ocean circulation and sea ice changes are expected to play a more important role than in inland regions. The AMO and PMO have similar contributions, and together they account for approximately 11% of temperature changes

during the period 850–1999. Although minor, the contribution is same as that from combined solar and volcanic forcing, indicating a similar importance of the AMO and PMO as solar and volcanic forcing on past temperature changes over East Asia.

The contribution of each driver is, however, not stable over time, and shows different values during the MCA, LIA and CWP. During the MCA, we found a more important role of internal climate variability (Goosse *et al.*, 2012), and we especially highlight the importance of the PMO, at least for East Asia. During the LIA, the importance of solar variability we found is somewhat larger than the findings from the NH temperature detection and attribution studies (Hegerl *et al.*, 2007; Schurer *et al.*, 2014). During the CWP, we suggest that the contribution of the internal variability related to the AMO is necessary to explain recent temperature changes in agreement with earlier works for the globe and NH (Steinman *et al.*, 2015; Stolpe *et al.*, 2017).

Our results suggest the relative contributions of the forcing factors to East Asian temperature changes vary between sub-periods, a similar phenomenon seen in the global mean temperature even for shorter (~15-35 years) intervals since AD 1891 (Folland *et al*., 2018). This implies the different contexts of external forcing may have different preferences to contribute or disturb the impacts of AMO and PMO. This inference is supported by our analyses of model simulation data (Ratna *et al*., in preparation), in which we found the AMO and PMO teleconnections with East Asian temperature show somewhat different patterns with or without the presence of external forcing.

Although we detected relatively important drivers over the MCA and LIA, the large proportion of temperature change over these periods still cannot explained by the factors we included in analyses. This suggests additional internal and/or external forcing factors, or non-linear feedback mechanisms, are needed for explaining the MCA and LIA, but reconstruction uncertainties may also come into play here. The uncertainty for the AMO and PMO reconstructions may be especially large because these reconstructions mostly rely on

teleconnections that, might not be stable over time (McAfee, 2017). Thus, we recommend caution in choosing reconstructions for climate variability modes, and in considering attributions for the AMO and PMO. In addition, our approach has limitations as it cannot consider nonlinear interactions between external forcing and internal variability and dynamic processes, and our results are subject to sampling variability especially for the CWP because this is the shortest period considered here. Future work should consider using climate model simulations (Ratna *et al*., in preparation) and a more sophisticated detection and attribution method (Hegerl and Zwiers, 2011) to complement our approach. Nevertheless, our approach has an important advantage that it incorporates internal variability via the observed or reconstructed climate modes such as AMO and PMO, which the models may not realistically simulate (see discussion in Folland *et al*., 2018).

**Acknowledgements**

J.W. is supported by the National Key R&D Program of China (grant: 2017YFA0603302), the National Science Foundation of China (NSFC; grant: 41602192), the Youth Innovation Promotion Association Foundation of CAS, and the CAS "West Light" Program. B.Y. is supported by the NSFC (grant: 41520104005, 41325008). T.J.O., B. Y., J.L., and J.W. are supported by the Belmont Forum and JPI-Climate, Collaborative Research Action 'INTEGRATE' (NERC grant: NE/P006809/1; NSFC grant: 41661144008). F.C.L. is partly supported by the Royal Swedish Academy of Letters, History and Antiquities, and the Bank of Sweden Tercentenary Foundation. H.Z and J.L. were supported from the German Science Foundation (DFG) project AFICHE. The reconstructions for East Asian temperature and climate forcings used in this study were obtained from the National Oceanic and Atmospheric Administration-National Centers for Environmental Information (NOAA-NCEI) for Paleoclimatology Data (https://www.ncdc.noaa.gov/paleo/). Our new composite reconstruction for East Asian temperature will also be made available from the NOAA-NCEI.

**References**

Ammann, C. M., F. Joos, D. S. Schimel, B. L. Otto-Bliesner, and R. A. Tomas (2007), Solar influence on climate during the past millennium: results from transient simulations with

the NCAR Climate System Model, *Proc. Natl. Acad. Sci. USA, 104*(10), 3713-3718.

Anchukaitis, K. J., et al. (2017), Last millennium Northern Hemisphere summer temperatures from tree rings: Part II, spatially resolved reconstructions, Quaternary. *Sci. Rev., 163*, 1-22.

Atwood, A. R., E. Wu, D. M. W. Frierson, D. S. Battisti, and J. P. Sachs (2016), Quantifying Climate Forcings and Feedbacks over the Last Millennium in the CMIP5-PMIP3 Models, *J. Clim.*, *29*(3), 1161-1178.

Berger, A. (1978), Long-term variations of daily insolation and Quaternary climatic changes, *Journal of the Atmospheric Sciences*, *35*(12), 2362-2367.

Bindoff, N. L., et al. (2013), Detection and attribution of climate change From global to regional, in *Climate Change 2013: The Physical Science Basis. IPCC Working Group I Contribution to AR5*, edited by T. F. Stocker, D. Qin, G.-K. Plattner, M. Tignor, S. K. Allen, J. Boschung, A. Nauels, Y. Xia, V. Bex and P. M. Midgley, pp. 867-952, Cambridge University Press, Cambridge, United Kingdom and New York, NY, USA.

Cheung, A. H., M. E. Mann, B. A. Steinman, L. M. Frankcombe, M. H. England, and S. K. Miller (2017), Comparison of Low Frequency Internal Climate Variability in CMIP5 Models and Observations, *J. Clim.*, doi: 10.1175/jcli-d-1116-0712.1171.

Chylek, P., J. D. Klett, M. K. Dubey, and N. Hengartner (2016), The role of Atlantic Multi-decadal Oscillation in the global mean temperature variability, *Clim. Dyn.*, *47*(9-10), 3271-3279.

Cook, E. R., P. J. Krusic, K. J. Anchukaitis, B. M. Buckley, T. Nakatsuka, M. Sano, and P. A. k. Members (2013), Tree-ring reconstructed summer temperature anomalies for temperate East Asia since 800 C.E, *Clim. Dyn.*, *41*(11-12), 2957-2972.

Crowley, T. J., and M. B. Unterman (2013), Technical details concerning development of a 1200 yr proxy index for global volcanism, *Earth Syst. Sci. Data*, *5*(1), 187-197.

D'Arrigo, R., and R. Wilson (2006), On the Asian expression of the PDO, *Int. J. Climatol.*, *26*(12), 1607-1617.

Dai, A., J. C. Fyfe, S.-P. Xie, and X. Dai (2015), Decadal modulation of global surface temperature by internal climate variability, *Nat. Clim. Change*, *5*(6), 555-559.

Esper, J., et al. (2012), Orbital forcing of tree-ring data, *Nat. Clim. Change*, *2*(12), 862-866.

Fang, K., E. Cook, Z. Guo, D. Chen, T. Ou, and Y. Zhao (2017), Synchronous multi-decadal climate variability of the whole Pacific areas revealed in tree rings since 1567, *Environ. Res. Lett.*, *13*(2), 024016.

Fisher, R. A. (1921), On the "probable error" of a coefficient of correlation deduced from a small sample, *Metron*, *1*, 3-32.

Folland, C. K., A. W. Colman, D. M. Smith, O. Boucher, D. E. Parker, and J.-P. Vernier (2013), High predictive skill of global surface temperature a year ahead, *Geophys. Res. Lett.*, *40*(4), 761-767.

Folland, C. K., O. Boucher, A. Colman, and D. E. Parker (2018), Causes of irregularities in trends of global mean surface temperature since the late 19th century, *Science Advances*, *4*(6), doi: 10.1126/sciadv.aao5297.

Frankcombe, L. M., M. H. England, M. E. Mann, and B. A. Steinman (2015), Separating internal variability from the externally forced climate response, *J. Clim.*, *28*(20), 8184-8202.

Ge, Q., Z. Hao, J. Zheng, and X. Shao (2013), Temperature changes over the past 2000 yr in China and comparison with the Northern Hemisphere, *Clim. Past.*, *9*(3), 1153-1160.

Goosse, H., E. Crespin, S. Dubinkina, M.-F. Loutre, M. E. Mann, H. Renssen, Y. Sallaz-Damaz, and D. Shindell (2012), The role of forcing and internal dynamics in explaining the "Medieval Climate Anomaly", *Clim. Dyn.*, *39*(12), 2847-2866.

Harris, I., P. Jones, T. Osborn, and D. Lister (2014), Updated high-resolution grids of monthly climatic observations-the CRU TS3. 10 Dataset, *Int. J. Climatol.*, *34*(3), 623-642.

Hartl-Meier, C., U. Büntgen, J. E. Smerdon, E. Zorita, P. J. Krusic, F. C. Ljungqvist, L. Schneider, and J. Esper (2017), Temperature Covariance in Tree Ring Reconstructions and Model Simulations Over the Past Millennium, *Geophys. Res. Lett.*, *44*(18), 9458–9469.

Hawkins, E., and R. Sutton (2009), The Potential to Narrow Uncertainty in Regional Climate Predictions, *Bull. Amer. Meteor. Soc.*, *90*(8), 1095-1108.

Hegerl, G., J. Luterbacher, F. González-Rouco, S. F. B. Tett, T. Crowley, and E. Xoplaki (2011), Influence of human and natural forcing on European seasonal temperatures, *Nat. Geosci.*, *4*(2), 99-103.

Hegerl, G., and F. Zwiers (2011), Use of models in detection and attribution of climate change, *WIREs. Climate Change*, *2*(4), 570-591.

Hegerl, G. C., S. Brönnimann, A. Schurer, and T. Cowan (2018), The early 20th century warming: Anomalies, causes, and consequences, *WIREs. Climate Change*, e522.

Hegerl, G. C., T. J. Crowley, M. Allen, W. T. Hyde, H. N. Pollack, J. Smerdon, and E. Zorita (2007), Detection of human influence on a new, validated 1500-year temperature reconstruction, *J. Clim.*, *20*(4), 650-666.

Imbers, J., A. Lopez, C. Huntingford, and M. R. Allen (2013), Testing the robustness of the anthropogenic climate change detection statements using different empirical models, *J. Geophys. Res.*, *118*(8), 3192-3199.

Kaplan, J., O., K. Krumhardt, M., E. Ellis, C., W. Ruddiman, F., C. Lemmen, and K. K. Goldewijk (2010), Holocene carbon emissions as a result of anthropogenic land cover change, *Holocene*, *21*(5), 775-791.

Kaufman, D. S., et al. (2009), Recent warming reverses long-term Arctic cooling, *Science*, *325*(5945), 1236-1239.

Knudsen, M. F., B. H. Jacobsen, M. S. Seidenkrantz, and J. Olsen (2014), Evidence for external forcing of the Atlantic Multidecadal Oscillation since termination of the Little Ice Age, *Nat. Commun.*, *5*, 3323.

Lean, J. L., and D. H. Rind (2008), How natural and anthropogenic influences alter global and regional surface temperatures: 1889 to 2006, *Geophys. Res. Lett.*, *35*(18), L18701.

Li, S., J. Perlwitz, X. Quan, and M. P. Hoerling (2008), Modelling the influence of North Atlantic multidecadal warmth on the Indian summer rainfall, *Geophys. Res. Lett.*, *35*(5), L05804.

Ljungqvist, F. C., P. J. Krusic, H. S. Sundqvist, E. Zorita, G. Brattström, and D. Frank (2016), Northern Hemisphere hydroclimate variability over the past twelve centuries, *Nature*, *532*(7597), 94-98.

Luo, F., S. Li, Y. Gao, N. Keenlyside, L. Svendsen, and T. Furevik (2018), The connection between the Atlantic multidecadal oscillation and the Indian summer monsoon in

CMIP5 models, *Clim. Dyn.*, DOI:10.1007/s00382-00017-04062-00386.

Luterbacher, J., et al. (2016), European summer temperatures since Roman times, *Environ. Res. Lett.*, *11*, 024001.

Mann, M. E. (2008), Smoothing of climate time series revisited, *Geophys. Res. Lett.*, *35*(16), L16708.

Mann, M. E., Z. Zhang, S. Rutherford, R. S. Bradley, M. K. Hughes, D. Shindell, C. Ammann, G. Faluvegi, and F. Ni (2009), Global signatures and dynamical origins of the Little Ice Age and Medieval Climate Anomaly, *Science*, *326*(5957), 1256-1260.

MacDonald, G. M., and R. A. Case (2005), Variations in the Pacific Decadal Oscillation over the past millennium, *Geophys. Res. Lett.*, *32*(8), L08703.

McAfee, S. A. (2017), Uncertainty in Pacific decadal oscillation indices does not contribute to teleconnection instability, *Int. J. Climatol.*, *37*(8), 3509-3516.

Meehl, G. A., A. Hu, B. D. Santer, and S.-P. Xie (2016), Contribution of the Interdecadal Pacific Oscillation to twentieth-century global surface temperature trends, *Nat. Clim. Change*, *6*, 1005-1008.

Miller, R. L., et al. (2014), CMIP5 historical simulations (1850–2012) with GISS ModelE2, *Journal of Advances in Modeling Earth Systems*, *6*(2), 441-478.

Newman, M., et al. (2016), The Pacific Decadal Oscillation, Revisited, *J. Clim.*, *29*, 4399-4427.

Otto-Bliesner, B. L., E. C. Brady, J. Fasullo, A. Jahn, L. Landrum, S. Stevenson, N. Rosenbloom, A. Mai, and G. Strand (2016), Climate Variability and Change since 850 CE: An Ensemble Approach with the Community Earth System Model, *Bull. Amer. Meteor. Soc.*, *97*(5), 735-754.

PAGES 2k Consortium (2013), Continental-scale temperature variability during the past two millennia, *Nat. Geosci.*, *6*(5), 339-346.

Schmidt, G. A., et al. (2012), Climate forcing reconstructions for use in PMIP simulations of the Last Millennium (v1.1), *Geosci. Model Dev.*, *5*(1), 185-191.

Schurer, A. P., G. C. Hegerl, M. E. Mann, S. F. B. Tett, and S. J. Phipps (2013), Separating forced from chaotic climate variability over the past millennium, *J. Clim.*, *26*(18), 6954-6973.

Schurer, A. P., S. F. B. Tett, and G. C. Hegerl (2014), Small influence of solar variability on climate over the past millennium, *Nat. Geosci.*, *7*, 104-108.

Shi, F., et al. (2015), A multi-proxy reconstruction of spatial and temporal variations in Asian summer temperatures over the last millennium, *Clim. Change*, *131*(4), 663-676.

Shi, F., B. Yang, and L. Gunten (2012), Preliminary multiproxy surface air temperature field reconstruction for China over the past millennium, *Sci. China. Ser. D.*, *55*(12), 2058-2067.

Sigl, M., et al. (2015), Timing and climate forcing of volcanic eruptions for the past 2,500 years, *Nature*, *523*, 543–549.

Steinhilber, F., J. Beer, and C. Fröhlich (2009), Total solar irradiance during the Holocene, *Geophys. Res. Lett.*, *36*(19), L19704.

Steinman, B. A., M. E. Mann, and S. K. Miller (2015), Atlantic and Pacific multidecadal oscillations and Northern Hemisphere temperatures, *Science*, *347*(6225), 988-991.

Stolpe, M. B., I. Medhaug, and R. Knutti (2017), Contribution of Atlantic and Pacific

Multidecadal Variability to Twentieth Century Temperature Changes, *J. Clim.*, DOI:org/10.1175/JCLI-D-1116-0803.1171.

Torrence, C., and G. P. Compo (1998), A Practical Guide to Wavelet Analysis, *Bulletin Am. Meteorol. Soc., 79*, 61-78.

Wang, J., B. Yang, and F. C. Ljungqvist (2015), A millennial summer temperature reconstruction for the Eastern Tibetan Plateau from tree-ring width, *J. Clim., 28*(13), 5289-5304.

Wang, J., B. Yang, F. C. Ljungqvist, J. Luterbacher, T. J. Osborn, K. R. Briffa, and E. Zorita (2017), Internal and external forcing of multidecadal Atlantic climate variability over the past 1,200 years, *Nat. Geosci., 10*(7), 512-517.

Wang, J., B. Yang, F. C. Ljungqvist, and Y. Zhao (2013), The relationship between the Atlantic Multidecadal Oscillation and temperature variability in China during the last millennium, *J. Quaternary Sci., 28*(7), 653-658.

Wang, S., X. Wen, Y. Luo, W. Dong, Z. Zhao, and B. Yang (2007), Reconstruction of temperature series of China for the last 1000 years, *Chin. Sci. Bull., 52*(23), 3272-3280.

Wilson, R., et al. (2016), Last millennium northern hemisphere summer temperatures from tree rings: Part I: The long term context, *Quaternary. Sci. Rev., 134*, 1-18.

Yang, B., A. Bräuning, K. R. Johnson, and Y. Shi (2002), General characteristics of temperature variation in China during the last two millennia, *Geophys. Res. Lett.*, *29*(9), 1324.

Zhang, H., et al. (2018), East Asian warm season temperature variations over the past two millennia, *Sci. Rep., 8*, 7702.

Zhou, J., and K.-K. Tung (2013), Deducing multidecadal anthropogenic global warming trends using multiple regression analysis, *J. Atmos. Sci.*, *70*(1), 3-8.

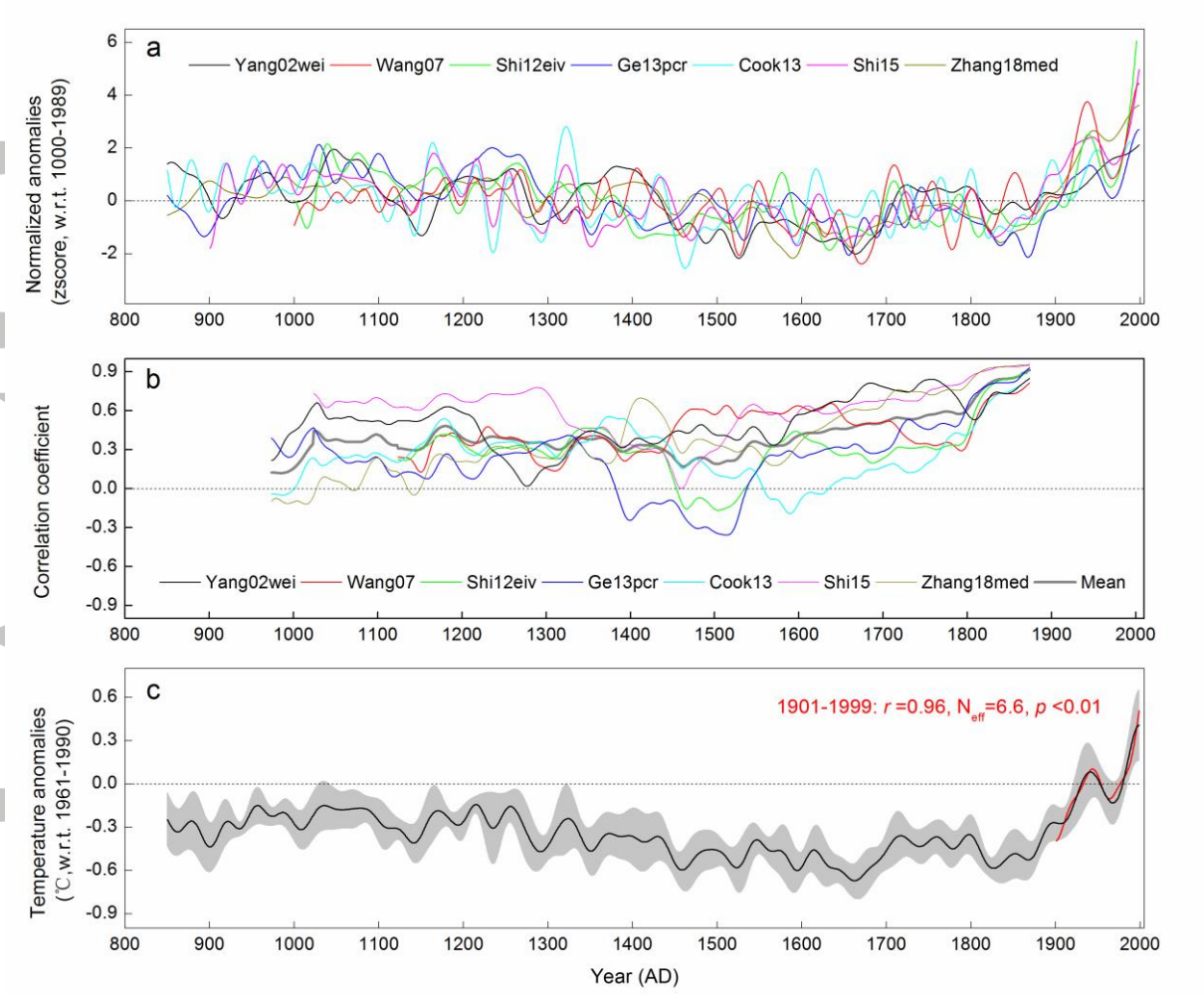


**Figure 1.** (a) The seven published millennia-long temperature reconstructions for East Asia, shown as 30-year low-pass filters and normalized anomalies. (b) The 250-year running correlation coefficients between each temperature reconstruction and the composite of other six reconstructions. Note that the Fisher transformation and its inverse function (Fisher, 1921) were used to calculate the mean of correlation coefficients in order to avoid the biases due to symmetrical sampling variability. (c) The scaled composite (black) and ±1 SD (shading) of the seven reconstructions and the CRUTS4.01 mean temperature for the extended warm-season over East Asia (red).

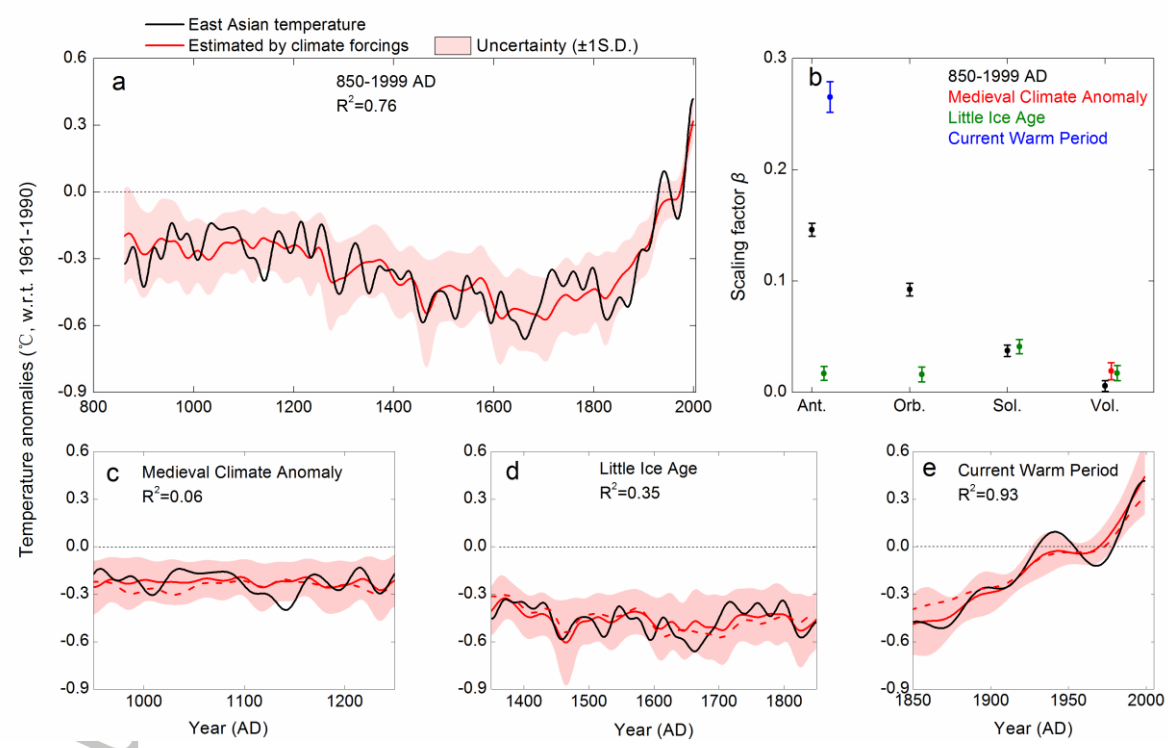


**Figure 2.** (a) The composite temperature reconstruction and the temperature changes attributed to radiative forcings by applying multiple linear regression (MLR) over the period 850–1999. The uncertainty range (pink shading) is the ±1 standard deviation (SD) of the attributed temperature time series when MLR is applied to the seven individual reconstructions rather than the composite reconstruction. (b) Beta values (scaling factor) and their 95% uncertainty ranges by individual climate forcing over the full period 850–1999, or separately over the Medieval Climate Anomaly (950–1250), Little Ice Age (1350–1850) and Current Warm Period (1850–1999). (c–e) Same as (a), but for the Medieval Climate Anomaly, Little Ice Age and Current Warm Period, respectively. Note that all forcing time-series are transformed to "z-scores" when performing the MLR in each case. This corresponds to the regression model of equation 1, and they only show scaling factors that are significantly different from zero. For each sub-period in panels (c), (d) and (e), the model fitted value over the whole time period is also added to show as red dotted lines.

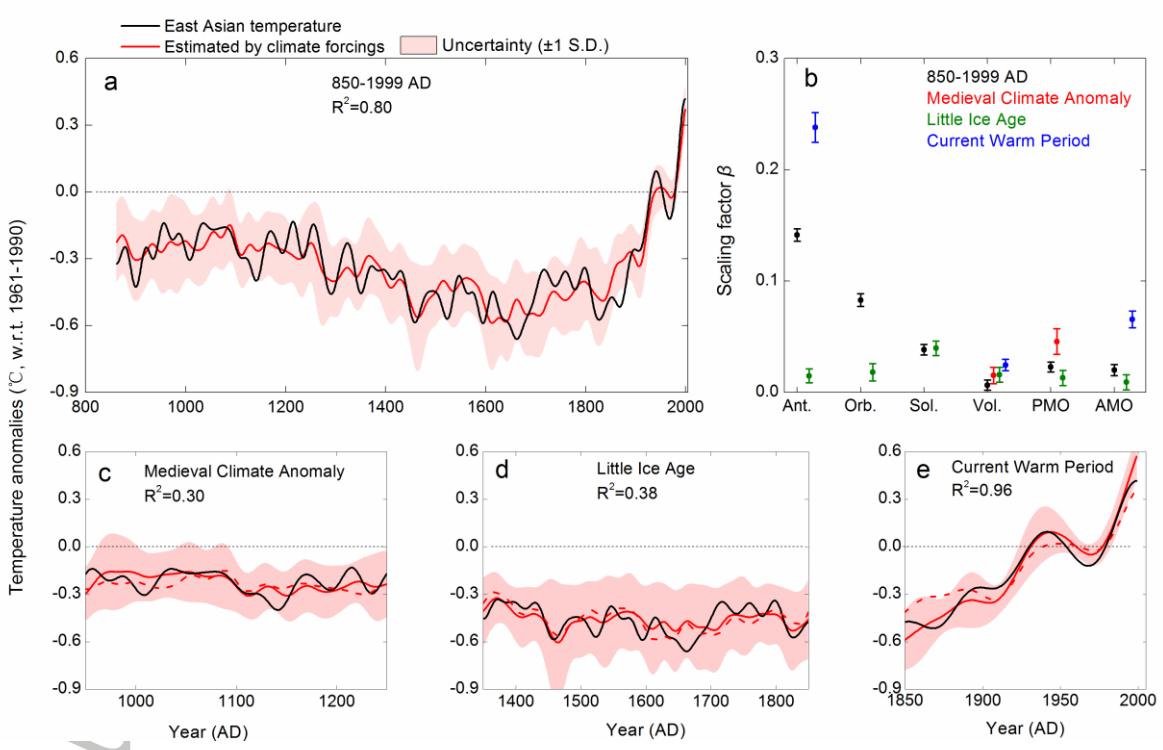


**Figure 3.** Same as Figure 2, but for the results when adding the AMO and PMO into the set of explanatory variables. This corresponds to the regression model of equation 2.

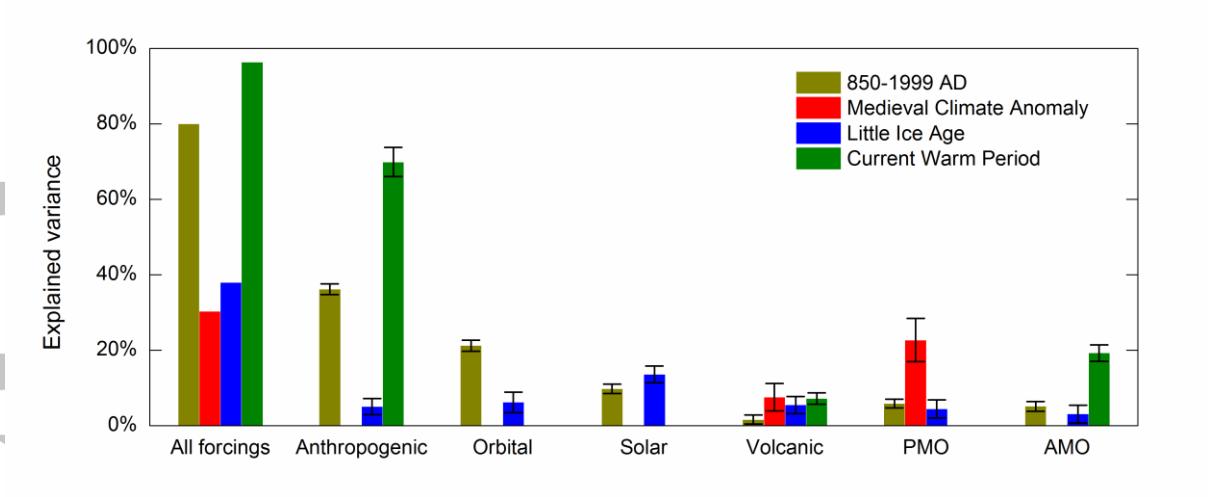


**Figure 4.** Variance (and its 95% uncertainty range) of the composite reconstruction that is explained by all climate drivers (external forcings and modes of internal variability) as well as by the individual drivers during the period 850–1999, Medieval Climate Anomaly (950–1250), Little Ice Age (1350–1850) and Current Warm Period (1850–1999).